Journal of Alloys and Compounds 514 (2012) 6–19

Contents lists available at SciVerse ScienceDirect

Journal of Alloys and Compounds

journal homepage: www.elsevier.com/locate/jallcom

Review

Mechanical properties of nano-silver joints as die attach materials

Kim S. Siow*

Package Innovation Development Centre, On Semiconductor SCG Industries Malaysia Sdn Bhd, Lot 122 Senawang Industrial Estate, 70450 Seremban, Negeri Sembilan, Malaysia

ARTICLE INFO

Article history:
Received 15 July 2011
Received in revised form 25 October 2011
Accepted 28 October 2011
Available online 7 November 2011

Keywords:
Mechanical properties
Sintering
Ag nanoparticles
Lead free die attach

ABSTRACT

This review traces the development of silver (Ag) as a die attach bonding material in the microelectronic packaging industry from its' early days as micron-scale silver flakes to the recent nanoscale Ag paste and other derivatives. Basic materials properties include the composition of Ag pastes, the methods of producing Ag nanoparticles, and product applications will be presented. Key processing conditions will be discussed to elucidate different factors which influence the mechanical properties of nano-Ag joints, principally the tensile and shear strength as well as thermal fatigue properties. Success in implementing nano-scale Ag pastes could only have been possible by deriving a fundamental understanding developed in the field of processing and using ceramic and metallic nano-powders.

© 2011 Elsevier B.V. All rights reserved.

Contents

1. Introduction 6
2. Micron-scale Ag flakes 7
3. Nano-scale Ag paste 8
 3.1. Synthesis of Ag nanoparticles 8
 3.2. Composition of nanoscale Ag paste 9
4. Mechanical properties 10
 4.1. Elastic modulus 10
 4.2. Strength 11
  4.2.1. Tensile strength 11
  4.2.2. Shear strength 12
 4.3. Factors affecting the bonding strength of nano-Ag joints 12
  4.3.1. Bonding pressure 12
  4.3.2. Sintering temperature 13
  4.3.3. Nanoparticle size, distribution and morphology 13
  4.3.4. Heating rate 14
  4.3.5. Dimension of bonding area 14
  4.3.6. Bonding substrate 14
  4.3.7. Sintering time 15
 4.4. Thermal fatigue properties 16
 4.5. Recent innovations in LTJT 16
 4.6. Future challenges in LTJT 17
5. Conclusions 17
 Acknowledgements 17
 References 17

1. Introduction

There are several European Union directives which aim to reduce and eventually remove lead from electronic materials because of its hazardous effect on human health. Examples of

* Tel.: +60 6 671 2155; fax: +60 6 678 0725.
E-mail addresses: kimshyong@gmail.com, kimshyong.siow@onsemi.com

0925-8388/$ – see front matter © 2011 Elsevier B.V. All rights reserved.
doi:10.1016/j.jallcom.2011.10.092

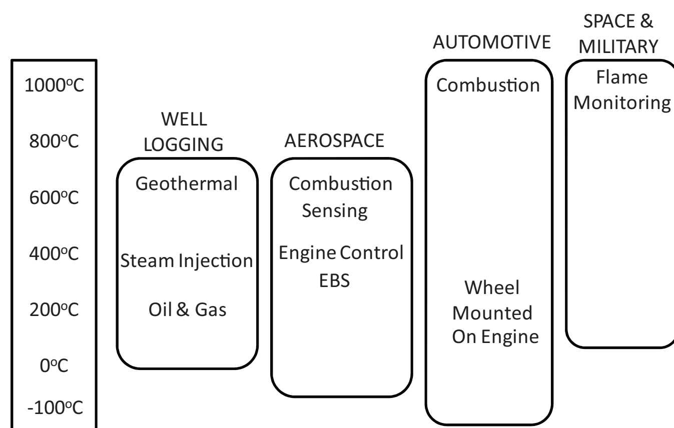

Fig. 1. Indicative temperature range [5].
Reprinted with permission; ©1999 IEEE

these directives are Restriction of Hazardous Substance (ROHS) 2002/95/EC, End of Life Vehicle (ELV) and Waste Electrical & Electronic Equipment (WEEE) 2002/96/EC. Pb–Sn die attach materials is exempted from these directives until 2014, but no efforts are spared to find Pb-free replacements for the die attach material. Current candidate solders like Bi-alloys, Zn-alloys, and Au–Sn alloys have many limitations like poor processability, poor corrosion resistance and high costs. These issues are comprehensively reviewed here [1–3].

Besides lead-free applications, another driver for evaluating alternative die attach strategies is the emergence of silicon carbide technologies to replace silicon technologies. In order to achieve higher performance, the former operates at significantly higher temperatures, power, and voltages than the latter [4]. Different segments of industries which utilize high temperature electronics are summarized in Fig. 1 with their operating temperature ranges [5]. Such high temperature applications require a new form of joining the dies to the chip-carrier or leadframe.

The low temperature joining technique (LTJT) has been proposed as a possible alternative to lead-free die attach materials and high temperature application mentioned above. LTJT is a technique pioneered by Schwarzbauer and others to produce die attach joints from micron-scale Ag paste for power electronics packaging in the late 1980s [6]. Since then, LTJT technology has garnered a great deal of interests amongst the academia as well as industry players based on more than 40 publications in this area for the period of 2010–2011.

There are numerous benefits associated with the use of Ag particles in LTJT. Silver has better thermal and electrical conductivities than the commonly used Sn–Pb or Pb-free joints. Nano-Ag joints are sintered at temperatures significantly lower than the melting temperature of Ag, typically 0.2–0.4 T_m [7]. Once sintered the Ag joint will have a melting temperature similar to bulk Ag (961 °C). This property will avoid the remelting problem in the downstream microelectronic packaging and assembly processes. Thermal impedance measurement also confirmed that nano-Ag joint perform better than Sn–3Ag–0.5Cu alloy or Sn–Cu–Ni–Ge alloy (better known as trade name "SN100C") [8]. Based on these properties, nano-Ag has been listed in recent literature as leading candidate for lead free die attach as well as die-attach for silicon carbide technologies [4,9–11].

Due to micron scale Ag flakes, the pressure required to affect this bonding in LTJT can be as large as 80 MPa [12] though lower pressures of ~10 MPa have also been demonstrated [6]. "Pressure sintering" is also a term commonly used to describe sintering of micron-scale Ag particles [13]. Pressure sintering is similar to the commonly used sinter-forging used in the ceramic industry but of even higher pressures in the range of more than 100 MPa [14]. In the semiconductor industry, pressure sintering was initially used in semiconductor components like diodes, thyristors, and insulated gate bipolar transistors (IGBT) that are more robust than the silicon trench technologies. Hence, there are various efforts to reduce the stresses impressed by the sintering conditions.

One viable approach for reducing the pressure requirement in LTJT is to reduce the size of Ag particles to the nanometer range [15,16]. When Ag particles are reduced to such a dimension the effective surface area, which in turn implies the number of Ag surface atoms increase several fold. The surface area may be as high as 23.81 m^2/g for Ag nanoparticles of 26 nm diameter [17]. These changes in surface area and concomitant increase in surface curvature provides the driving forces to sinter with neighbouring Ag atoms at temperatures 0.2–0.4 of the melting point (T_m) [7]. Due to the use of nano-size particles LTJT is also known as nanocrystal-enabled solid state bonding [18].

This review traces the early development of LTJT with micron-scale Ag flakes. Early lessons from the formulation of the micron-scale Ag paste and processing routes eventually led to the development of nanoscale Ag pastes. Different processing parameters affecting the mechanical properties like shear strength, tensile strength, elastic modulus, fatigue properties of nano-Ag joints are discussed. Key lessons are drawn from results related to Ag nanoparticles used in LTJT and guiding principles are also taken from related fields like Ag nano-ink of printed electronics and other metallic or ceramic nanoparticles. This review is expected to be useful to researchers who are exploring nano-scale Ag pastes as options for lead-free die attach materials.

2. Micron-scale Ag flakes

Early effort in the use of micron-scale Ag flakes as joining materials is led by Schwarzbauer and his team. Several patents have been filed in the area of process, materials applications and component level joining with the micron-scale Ag paste [13,19]. In general, the processing steps are [13,20–22]:

1. Print the micron-scale Ag paste (Ag flakes, carrier and solvent) on the board.
2. Preheat the micron-scale Ag paste to drive out the solvent.
3. Place the die on the dried Ag paste.
4. Sinter the die under pressure (9 MPa) and high temperature (150–250 °C) to form the Ag bond.

Other researchers have applied and preheated this micron-scale Ag paste on the wafer backside before the sawing and die-bonding stage [23]. Another approach for applying micron-scale Ag paste was to create the microscopic Ag particles in situ for bonding by reducing the Ag oxide chemically prior to die-bonding [24].

However, there were claims that the preheating stage can be eliminated if a slow heating rate of less than 2 °C/min was maintained to reach the sintering temperature of ~180 °C [25]. This non-pre-heating approach was based on the sintering of Ag flakes at their edges to form an extended network of metal flakes in the absence of applied pressure [25]. Others also removed the preheating stage but sintered the micron-scale Ag paste in an oxidizing environment at 300 °C [26]. Other used pre-sintered micron-scale Ag laminates to enable bonding of electronic component at lower temperature (150 °C) and pressure (30 MPa) [27].

These micron-scale Ag pastes consist of two main components namely Ag flakes (diameters of ~15 μm)[13,27] and solvents like cyclohexanol [12,13], butanol [25], terpineol [28], or an ethylene glycol ether [28] mixture of cyclohexanol–methanol [27]. In the printed electronics industry metal-organic compounds like silver

stearate or silver oxalate are often added to be decomposed to form the silver bridge linking the micron-scale silver flakes [29]. Such an approach can also be used in the formulation of micron-scale Ag flakes as bonding materials but is not found in the literature.

Since this early success of micron scale Ag paste in component level mounting, there is an interest to use Ag paste to bond other silicon technology die to the substrate materials; aptly termed as "die-bonding". A good "die bonding" step must fulfil certain requirements such as not transmitting destructive stress to the silicon dies during bonding and operation, ability to withstand extreme temperature without degradation in bonding quality, good electrical and thermal contact between the silicon die and substrate materials.

3. Nano-scale Ag paste

In the development of ceramic or metallic nanoparticles, consolidation or compaction was always carried out before sintering but this processing route was only meant for making bulk materials with desired thermo-mechanical properties [14], not for bonding materials as described here.

Adaptation of this approach in nanoscale Ag paste is limited and may result in undesirable effects. Compaction of these dried and porous nano-Ag pastes before sintering may not be a feasible approach to achieve higher densities because Ag nanoparticles have a large number of particle–particle contacts per unit volume which creates high internal stress [30]. This residual strain is likely to cause delamination between the dried nano-Ag paste and the frame. On the other hand, foams of dried Ag paste have been reported to adhere easily to smooth surfaces like silicon and polyimide [28] though the bonding requires other processing conditions which will be discussed later.

In general, the process steps of using nanoscale Ag paste were quite similar to that of micron-scale Ag paste [31–34]. There were also some reports which describe a different approach compared to micron-scale Ag sintering-eliminating the preheating stage before the die attachment step [35–42]. The heating rate is very critical to drive out the solvent and promote sintering simultaneously, details of which will be discussed in later sections. Others applied and baked this nanoscale Ag paste on the backside of the wafer before die bonding on the leadframe [43]. Another variation is to apply and dry the nanoscale Ag paste on the wafer and the leadframe to ensure metallurgical bonding and mechanically stable anchoring of the porous dried nanoscale Ag paste during die bonding [40,43].

Typically, nanoscale Ag paste is transferred to the substrate by spray coating, foil transfer, dispensing [44], stencil or screen printing [31] and dipping [43].

Each variation of the process steps mentioned earlier is expected to influence the sintering mechanism and the final mechanical properties of the nano-Ag joint. These variations are expected to affect the two primary stages of joint formation namely the evaporation of solvent and the accessibility of oxygen to remove the dispersant on the Ag nanoparticles to allow the sintering process to proceed [35,45,46]. Some researchers introduced a third stage in the process flow, adding a final burn-off of the higher molecular weight binder system [47]. These different stages will be discussed in detail in the subsequent section on factors influencing shear strength of nano-Ag joints. Depending on the type of dispersant used in the Ag nanoparticle materials, exothermic peaks were detected between ~220 °C and ~280 °C during sintering of Ag nanoparticles. These peaks could be attributed to thermal events such as [48]:

1. Crystallization and consolidation of the metal particles.
2. Recrystallization of strained metal particles.
3. Diffusion between unstable surface atoms on the nanoparticles which leads to surface sintering.
4. Gas phase formation/evolution from the nanoparticles.
5. Oxidation of chemisorbed fatty acids (carriers or solvents) [31].

While each of these thermal events has equal probability to cause the sintering of nanoscale Ag paste, its intensity may differ depending on the bonding routes described earlier, the materials and physical properties of the Ag nanoparticles and type of dispersants.

Generally, there are three stages of sintering for nanopowders although the morphological transition from one stage to another is not always well defined [14,16,49]. In the initial stage of sintering the adhesion mechanism, like surface diffusion, dominates to produce necking at adjacent Ag nanoparticles [50] with a corresponding increase in mechanical strength [14]. At this stage of sintering, the ratio of X/D is less than ~0.3 where X is the particle–particle neck size and D is the particle (grain) size [49].

In the intermediate stage the networks of interpenetrating pores are shrinking in the radial direction with a concomitant increase in density up to 90–92% of theoretical [14,49]. The "X/D" is more than ~0.3 at this stage of sintering [49]. In the final stage there will be collapse of tubular pores to spherical pores [49]. Under the right sintering conditions, all pores are eliminated [14]. For metallic nanoparticles, the large shear stress at the curved neck regions also generates dislocations which induce grain rotation which aids in densifying the sintered nanoparticles [51].

3.1. Synthesis of Ag nanoparticles

The earliest record of producing unpassivated Ag nanoparticles or colloidal Ag, as they were known, was documented by Frens and Overbeek in 1969 based on the Carey Lea's approach of 1889 [52]. Since then, there have been numerous reviews on the synthesis of Ag nanoparticles for diverse applications like electronics, green technologies, biomedical needs, etc. [53–55]. This review gives a short summary of available techniques with emphasis on synthesis of Ag nanoparticles to formulate Ag paste for die attach application. Generally, the Ag nanoparticles of sizes less than 20 nm are precipitated from Ag salts to form agglomerates with sizes ranging from 800 to 3500 nm [31]. Reducing agents like ascorbic acid [40,56], hydrazine monohydrate [57], sodium citrate [58] or sodium citrate dihydrate [59], polyvinylpyrollidone [50], ethylenediaminetetraacetic acid (EDTA) [60], sodium sulfite [61] and sodium borohydride [62] were added into Ag salts like nitrates, sulphates or chlorates or Ag–ammonia complexes [62]. The reducing reaction occurred in a polar solvent such as ethanol, methanol, acetonitrile or tetrahydrofurane [40]. Condensation with a centrifuge might be carried out after the reduction steps to increase the concentration of the Ag nanoparticles [58].

Besides precipitation techniques, combustion chemical vapour condensation (CCVC) also produced unpassivated Ag nanoparticles from $AgNO_3$ [48]. In the CCVC process, precursor containing Ag-bearing chemical were dissolved in combustible fuel. The Nanomiser® Device atomized this precursor into microscopic droplets in an oxygen stream which were then combusted to produce the Ag nanoparticles. Others used a thermal decomposition method to produce a passivating layer in situ by mixing and heating $AgNO_3$ with fatty acids like oleic acid, stearic acid and myristic acid in a nitrogen atmosphere [63]. Monodispersed Ag nanoparticles could also be produced by reacting silver myristate or silver tetradecanoate ($C_{13}H_{27}CO_2Ag$) with a tertiary alkylamine like triethylamine [64] or trioctylamine [65]. This technique used the carboxylate ligand precursor to prevent aggregation and control the size distribution while the amine reduced amine-coordinated intermediates to Ag nanoparticles [65]. The oxidation of long chain

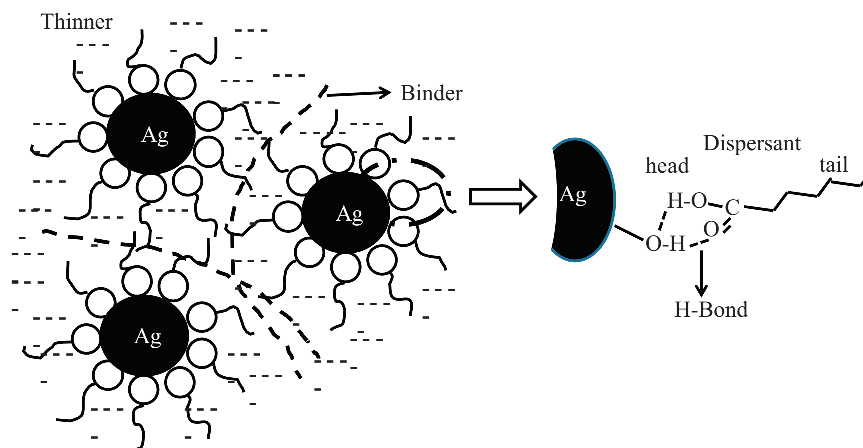

Fig. 2. Functions of the dispersant, binder and thinner in the formulation of nanoscale Ag pastes [16].

alcohols with Ag_2CO_3 also produced passivated Ag nanoparticles [35].

3.2. Composition of nanoscale Ag paste

The weight percentage of Ag nanoparticles in the nanoscale Ag paste is normally above 50% with percentages as high as ~70% [38] or ~80% [40]. This percentage will ensure its viscosity is suitable for applying the die attach materials via screen printing or dispensing methods. Unlike highly conductive epoxies, nanoscale Ag paste forms an interconnect material of "100% Ag".

Besides Ag nanoparticles, the main additives of nanoscale Ag paste are dispersants, binders and solvents [16]. Most literature treats the dispersant and binder as having the same functions and uses the two terminologies somewhat interchangeably. Besides dispersing the nanoparticles, binders have the additional function of preventing cracking of the dried Ag paste during handling [16]. Solvent is also added to the nanoscale Ag paste to adjust viscosity for easy printing after the initial blend of Ag nanoparticles and binders-dispersants are made. Examples of these additives are shown in Table 1 [66–68].

Dispersants, as shown in Fig. 2, consists of polar acids which anchors on the Ag nanoparticles while the hydrophobic tails act as spacers from adjacent particles [16]. This dispersant provides steric resistance and decreases the system energy to prevent the nanoparticles from melting and self-sintering [69].

Experimentally, self-sintering of Ag nanoparticles (known as "submicron Ag") at room temperature had been deduced with reduction of surface area using BET adsorption isotherm as early as 1984 [70]. However, aggregation or agglomeration of Ag nanoparticles can also contribute to the reduction of the total surface area. In recent times, the emerging interest of printing electronic circuits at room temperature spurred microanalytical activities in this area. HR-SEM (high resolution scanning electron microscopy) and in situ TEM (transmission electron microscopy) analyses were able to demonstrate self-coalescence of Ag nano-particle at ambient temperature [71,72].

Aggregates and agglomerates of nanoparticles are differentiated by the strength of the interparticle bonding [14]. Agglomerates can be reverted to nanoparticles by ultrasonic or mechanical agitation while the same cannot be carried out for Ag aggregates.

The selection of a dispersant depends on the effectiveness in dispersing Ag nanoparticles and reaching the desired sintering temperature in the shortest time possible. Dispersants constitute between ~1 and ~15 weight percent of the total weight of passivated Ag nanoparticles [33] although the percentage of all organics in the paste could be as high as 22 weight percent [16]. It is important to adequately protect these Ag nanoparticles from self-coalescence until the sintering temperature is reached because agglomeration or aggregation at lower temperatures will reduce the driving force for densification during the sintering step.

Some dispersants like fatty acids with longer hydrocarbon agents could disperse the Ag nanoparticles better than those with shorter hydrocarbon chains [16]. Others specified the dispersant from the perspective of molecular weight to be less than ~250 g which is a relatively long hydrocarbon [40]. Longer chain dispersants increase the steric repulsion because of unfavourable entropy in the confined, highly curved spaces between Ag nanoparticles [73]. The magnitude of steric repulsion was also affected by the solvent used in the paste which influenced the radius of gyration of these dispersant and other binders in the paste [73].

The targeted burnout temperature of the dispersant is directly related to its boiling temperature. As shown in Fig. 3, the boiling point of the dispersant is related to the number of carbons in the dispersant [16]. Hence, it is possible to choose a dispersant which will decompose just below the sintering temperature of the nanoscale Ag paste. In this respect, polyvinylpyrollidone (PVP) had been found to be unsuitable because of its' high temperature stability up to and above ~300 °C [45].

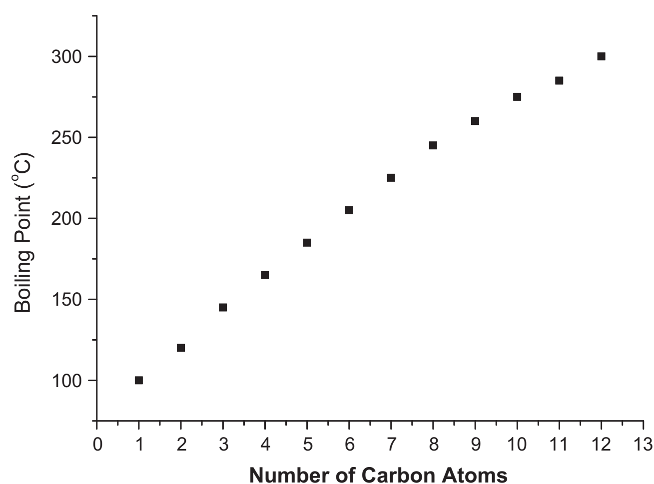

Fig. 3. The relationship of the boiling point of fatty acid versus their number of carbon atoms.
Adapted from the Sigma–Aldrich websites [16].

Table 1
Main additives of nanoscale Ag paste.

No	Component	Example
1	Dispersant/passivating layer/organic shell/capping agent	Menhaden fish oils [16,67], poly(diallydimethyl ammonium chloride) (PDDA) [16,67], polyacrylic acid (PAA) [16,67], polystyrene sulfonate (PSS) [16,67], triethylene glycol [32], methyloctylamine [40,56], dodecylamine [66], hexadecylamine [33], myristyl alcohol [46], 1-dodecanol [35], 1-decanol [35] stearic acid, oleic acid, palmitic acid [31], dodecanethiol [33]
2	Binder	Ethyl cellulose [68], polyvinyl alcohol [16], polyvinyl butyral (PVB) [16,67], wax [16,67]
3	Solvents/thinner	Isobornyl cyclohexanol (IBCH) [36], texanol [16,67], terpineol [16,40,41,67], butyl carbitol [33], toluene [33], xylene [40], ethanol [40], phenol [40].

Therefore, an ideal dispersant possesses low binding energies to Ag nanoparticles surfaces and a low boiling temperature to ensure its easy evolution. At the same time this dispersant must be stable during extended room-temperature storage. This dispersant ideally decomposes in a relatively narrow temperature band in a non-oxidizing environment below 300 °C. A non-oxidizing environment is also preferred to avoid oxidizing the substrates and surfaces used in die bonding.

In certain circumstances, additional surfactants such as BYK163 and Dysperbyk 163 were added to disperse the Ag nanoparticles [33]. Then the mixture of different additives and Ag nanoparticles were mixed in a high speed mixer before ball-mill or 3-roll mill into a homogeneous phase [33]. Others used ultrasonic agitation and vacuum evaporation to mix the nanoscale Ag paste [16].

Besides blending nanoscale Ag paste, others used Ag nanoparticles inks from printed electronics as bonding materials to form nano-Ag joints [18]. Although nano-Ag inks have some similarities in selection of dispersants and solvent vehicles with the nanoscale Ag paste their final compositions are dissimilar [74]. In the literature, the nano-Ag ink is typically used to fabricate conductive lines under pressureless sintering and seldom reported as die attach materials.

Due to oxidation, and in certain cases by formulation, Ag oxide particles will be present in Ag nano-ink or nanoscale Ag paste [18,75,76]. Their effect on the bonding qualities will be discussed in subsequent sections. Others include Ag_2CO_3 or silver lactate as reactive materials to be decomposed to reactive Ag to fill the porosity in the nano-scale Ag paste [41,76]. Such approaches have been reported earlier to bind adjacent micron-scale silver flakes with silver decomposed from metal-organic silver compounds like silver 2-ethylhexanoate or silver oxalate [29].

Alternatively, Ag pastes containing exclusively silver compounds like silver lactate or Ag_2CO_3 have been claimed to be a better approach to form interconnects than Ag paste mixtures of metallic silver nanoparticles because the former has less problems of agglomeration which generally increases the sintering temperature [76]. Compounds of Ag_2CO_3 have also been detected as residuals during processing of nano-Ag paste from $AgNO_3$ and sodium citrate [58] or even in the colloidal Ag particles produced from electric spark discharge technique [77].

Other impurities like copper, potassium and sodium are also typically found in the nanoscale Ag paste in the range of less than 1000 ppm, although it has been reported on rare occasion that the copper content may rise to ~2700 ppm [31]. Sodium or potassium salts of the fatty acids which were used as lubricants for the milling process, were also detected in the Ag paste [31]. These impurities did not appear to interfere with the bonding process [31] but instead it had been shown to improve bondability of the Ag paste to the copper substrate [38].

4. Mechanical properties

Unlike Sn–Pb solders, Ag joints do not suffer from room temperature ageing because of the low homologous temperature of $\sim 0.3T_m$. Sintered nano-Ag joints assume the melting temperature of bulk Ag (961 °C) after formation. Its low homologous temperature also results in insensitivity to strain rate and hence, creep is not expected to have a marked influence on the mechanical properties of the joint material at room temperature. However, reduction of tensile strength for sintered bulk nano-Ag has been reported to be significant at strain rate of $0.001\%s^{-1}$ and testing temperature of more than 120 °C [78].

4.1. Elastic modulus

Elastic modulus is the ratio of stress to strain in the elastic region during a tensile loading. Elastic modulus is essentially independent of small compositional or microstructural differences because it depends predominantly on forces between atoms in the crystal lattice. In the case of sintered Ag nanoparticles the microstructure and composition is almost homogeneous except for residual dispersant.

In the literature, the elastic modulus (E) of free-standing sintered Ag nanoparticles, as measured by tensile testing and dynamic mechanical analyser, was reported to be ~9 GPa [15] and ~ 6–7 GPa [78,79] respectively at room temperature. By comparison the elastic modulus for sintered Ag nano-ink and sputtered Ag were 118 GPa [80] and 148 GPa [81] respectively (N.B. Elastic constant of a typical bulk silver is 82.7 GPa [82].) The latter measurements were carried out with a nano-indenter in compression mode. In the case of free-standing sintered Ag nanoparticles, the sintering was carried out when the nanoscale Ag paste was constrained by a substrate [15]. Hence, the test piece was likely to be more porous than usual which further lowered the elastic modulus.

Besides the density of pores the ratio of "annular flaw size/pore radius" also influences the elastic modulus of nanomaterial primarily in compacted nanoparticles [83]. This concept can be traced to the stress distribution at the sharp pore tip. A larger ratio implies that the crack is longer and sharper resulting in a higher stress concentration. The joint will experience brittle failure in the absence of any stress relaxation mechanism. However, a close examination of published stress–strain curves of nano-Ag joints [84] showed the minimum macroscopic yield before failure and localized yield as exemplified by dimple formation on the fracture surfaces.

In the case of the shear modulus (G), values ranging from 0.4 to 0.6 GPa were derived from published shear stress–strain graphs of nano-Ag sintered joints [84]. In a related study, if the sound wave velocity measurement method was used to measure compacted Ag nanoparticles (97% density), the effective elastic constant was approximately 20% lower than those reported for polycrystalline Ag ≈ 66 GPa (E) and ≈24 GPa (G) [30]. The researchers' analysis attributed the cause of this observation to the indirect influence of internal stress in the Ag compact while dismissing the influence of disordered interfacial structure and intergrain sliding in this compacted Ag nanoparticle material. It should be mentioned that this Ag compact was not sintered but merely compacted at 2.3 GPa.

In summary the modulus of printed and sintered Ag nanoparticles (6–9 GPa) [15,78,79], which are lower than moduli of typical Pb–Sn, or Pb-free, solder joints provides good thermo-mechanical properties during thermal cycling [85]. This low modulus is entirely

fortuitous and a result of sintering of un-compacted Ag nanoparticles.

It is neither practical nor the aim of current research trends to produce a nano-Ag joint of 100% density because of the need to balance the elastic modulus and other mechanical properties like strength and fatigue properties [85]. High density Ag nanoparticles like those in compacted Ag achieving densities from 85% to 97% are also likely to face grain-growth issues which reduce the good mechanical properties of nanocrystalline Ag [30,86]. Elsewhere, it has been reported that nanomaterials with 90% density and open pores morphology is the most convenient way to control grain growth in nanomaterials [7].

4.2. Strength

There are two types of strengths: bulk sintered Ag nanoparticles and nano-Ag joint strength. Two possible loadings namely shear and tensile, are possible. Bulk sintered Ag nanoparticles can only be tested in tension. This bulk strength forms the minimum strength of the joints if the interfacial bonding with the substrate is high. In one study, the bulk tensile strength for Ag nanoparticles sintered at 280–300 °C was −43 MPa [15]. Based on the published stress–strain graph there was minimal strain hardening and the yield strength was estimated to be 30 MPa (0.02% offset) [15]. These tensile and yield strengths are comparable to the tensile strength of Pb-free solders reported in the literature [87].

However, the yield strength of sintered nano-Ag was comparatively lower than compacted Ag nanoparticles based on hardness testing converted yield strength of about 200 MPa, based on the following formula: yield strength is ∼1/3 of the hardness (in GPa) [30]. This result is to be expected because of the higher porosity in the sintered nano-Ag joint versus the compressive loading in the hardness tester which tends to close the pores.

4.2.1. Tensile strength

During tensile loading of a joint, the cross-section of the sample contracts to maintain the volume of the Ag nanoparticles, and void volumes alter their shape accordingly. This contraction is constrained by the substrate which transfers the uniaxial tensile stress into triaxial stress within the joints [88]. The adjacent substrates are still stressed within elastic range. As a result the joints will only fail when they reach the brittle fracture stress point of the bonding material. This transfer of stress will elevate the measured tensile strength above bulk values of the bonding materials. Surprisingly, when the tensile strength of a nano-Ag joint [32] was compared to that of bulk sintered Ag nanoparticles [15], the tensile strength of the former was lower than the latter. This difference is likely to be caused by the efficient transfer of stress in brazed joints [88] compared to the poorer transfer in the relatively low density sintered nano-Ag joint.

As shown in Fig. 4, a higher sintering temperature produces a joint of higher tensile strength [32,89]. A similar observation was recorded for the shear strength in Fig. 5 for joints which have been fabricated under similar bonding pressures [37,38,46,56]. A higher percentage of dispersant on the Ag nanoparticles will decompose at a higher sintering temperature. This decomposition exposed the unpassivated Ag nanoparticles to neighbouring nanoparticles for coalescence [32]. The resulting nano-Ag joint formed strong bonds and the fracture interfaces were reported to be cohesive failure through the sintered Ag nanoparticles [32]. As shown in Fig. 4, the joint design also influences the increase of tensile strength at similar sintering temperatures [58]. Hu's design of using Cu wire bonding to Cu pad design resembled mixed "tensile-shear" stress [58] instead of the relatively "pure" tensile stress used by Akada et al. [32] and Hirose et al. [89]. Their dispersant chemistries are also likely to be different and its influence on the tensile strength

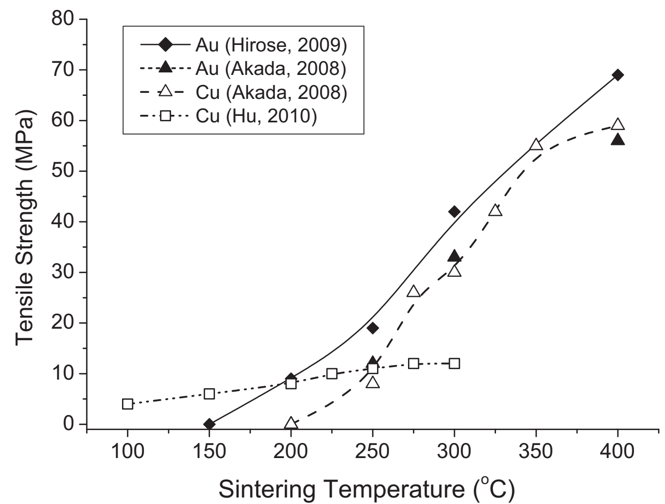

Fig. 4. Tensile strength of Ag nanoparticles joints on copper (Cu) and gold (Au)-plated substrates at 5 MPa, 5 min [32,58,89].

will be discussed later. It should be noted here that when the sintering temperature of nano-Ag paste, used by Hu et al., was increased to 250 °C, the failure interface shifted to substrate breakage instead of joint failure [58].

There is some speculation that the decomposition of Ag oxides to Ag also contributes to the sintering process at higher bonding temperatures. Different decomposition temperatures of Ag oxides such as 210 °C [75], 250 °C [86,90], 280 °C [18], 330 °C [91], 385 °C [92], 454 °C [93] have been reported in the literature. The exact decomposition temperature and mechanism of Ag oxides to Ag depends on several factors like the preparation method of the Ag oxide particles, different analysis methods, mechanical ageing conditions, partial pressure of gases like oxygen or CO_2 [92–94]. Regarding testing methods, dynamic heating methods with differential scanning calorimetry (DSC) and thermo-gravimetric analyser (TGA) normally produces a higher decomposition temperature, as much as 50 °C more than isothermal heating methods, which is followed by phase identification with X-ray diffractometer (XRD), Raman spectroscopy or Fourier transform infra-red (FTIR) spectroscopy [93].

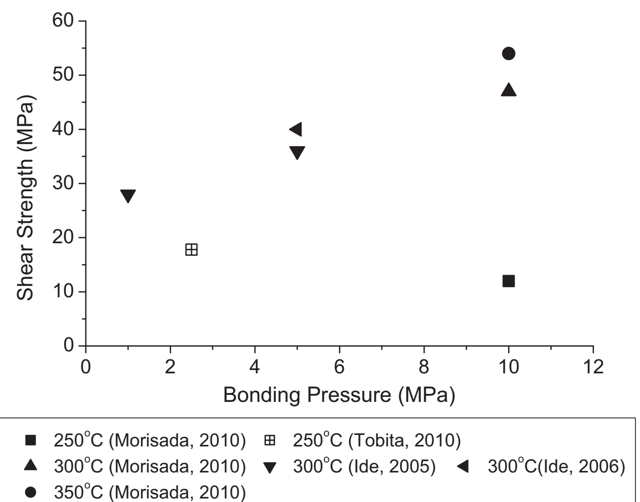

Fig. 5. Shear strength of Ag nanoparticles joints for bonding in ambient atmosphere for Ag nano-particle size between 8–11 nm using "double-copper disc" configuration [37,38,46,56]. *Note*: "250 °C", "300 °C" and "350 °C" refer to the sintering temperature for this joint.

An examination of published DSC and TGA data of Ag nanoparticles did not reveal any thermal activity related to the decomposition of Ag oxides in the temperature range above ∼350 °C [31,48,56,68,89]. Hence, the influence of decomposition of Ag oxides, if any, on the sintering of Ag nanoparticles is likely to be minimal. Silver nanoparticles, per se, had also been reported to reduce the burnout temperature of the binder to a range below ∼350 °C [68].

4.2.2. Shear strength

The loading for die attach application is often in shear mode during thermal cycling. Microscopically, yielding mechanism of a metallic system like sintered Ag nanoparticles is crystal planes slip which is controlled by shear stress. In shear loading, deformation occurs within the bonding material which is likely to produce more repeatable results. However, deformation during sample preparation could introduce a tensile mode into the pure shear loading resulting in a saturation of the maximum shear strength at values lower than the actual strength, to approximately 40 MPa for one particular joint design reported in [95].

The most common approach adopted to measure the shear strength of nano-Ag joint is to use a fixture similar to a commercial die shear tester to shear a "square/rectangle" bonded onto a frame, or two coins with "face to face" bonding. This tester consists of an instrument to apply the load with a contact tool to shear the "silicon die" at lift-off offset from the joining substrate. This approach requires the contact tool and dies to be kept parallel to each other to avoid cracking the dies before shearing occur. Another concern with such a die shear tester is the lift-off offset from the joining substrate. Current approach normally uses this joining substrate as the datum but uneven thickness of the nano-Ag joint can result in peeling of the die attach materials. Several standards like IPC-TM-650 and MIL-STD 883 provide some guidelines for die shear testing and loading.

A single lap shear joint has also been reported to measure the shear stress of nano-Ag joints [44,68], but it suffers from the addition of a bending component. The bending introduces a peeling stress into the total stress measurement which thereby underestimates the actual shear stress. The length of joint overlap also influenced the measured shear strength [88]. With increasing length of overlap, the shear strength was found to decrease because the central portion of the joint sustained little or no stress, while stress was concentrated at both ends. Such geometric factors must be taken into consideration when comparing results from different sources.

4.3. Factors affecting the bonding strength of nano-Ag joints

4.3.1. Bonding pressure

The influence of bonding pressure on the shear strength is illustrated in Fig. 5 for shear testing on copper substrates. Besides the results for a sintering temperature of 250 °C, it is apparent from Fig. 5 that increasing the bonding pressure will result in higher shear strength for nano-Ag bonded with copper substrates [37,38,46,56]. A similar trend was reported for joints formed on Ag-plated substrates [68].

When pressure is applied during sintering, the hydrostatic pressure and shear stress build-up in the nano-Ag joint is similar to that built-up in sinter forging of nanocrystalline ceramics without die (no lateral constraints) [49]. The hydrostatic component increases the average number of contacts between Ag nanoparticles to increase the sintering rate [68,95]. If the amount of pressure is sufficiently high, the induced shear strain will also tend to close the pores and align the grains similar to those reported in nanoceramics [49]. As a result the path for diffusion and the driving force for sintering also increase concomitantly [68,95].

However, most published results in literature, including those reviewed here, show extensive porosity suggesting that pressure and other sintering conditions like temperature and time were not consolidating the nano-Ag to a high density. Earlier in Section 4.1, the author has discussed the need to have a porous nano-Ag joint with lower elastic modulus for enhanced reliability in thermal cycling application. In this section, sufficiently high density is needed to achieve reasonable strength to meet the loading requirement of the nano-Ag joint. Hence, a balance must be struck between these two objectives.

In Fig. 5, the sintering pressure for various bonding experiments was applied for duration of 150–300 s. During this time it is likely that the higher pressure is only effective if an elevated temperature, higher than 250 °C to oxidize the dispersants, is achieved. Similar observations of "high temperature to achieve better sintering properties" have been reported for nano-ceramic system like trialuminides [96].

In order to ease the automation of die-bonding, there have been several attempts to sinter the nanoscale Ag paste without the addition of pressure [35,39,68]. Such approaches are known as "pressureless sintering" in the field of nanocrystalline ceramics which typically control sintering schedules like sintering/heating rate and combined-stage sintering [49]. Some of these approaches have been adopted in forming nano-Ag joints, and will be discussed later [39,68].

Although the shear strengths for pressureless sintering were adequate, i.e. 11–12 MPa, the fracture surface suggested uneven bonding with weak spots scattered on the joining areas [35]. In the absence of applied pressure the sintering mechanism was likely to be assisted by liquid capillary pressure from the "molten" surface of the nanoparticles [36]. The melting temperature of Ag nanoparticles with a dimension of 2.3 nm can be as low as ∼360 °C [97] while its surface may melt at lower temperatures [98]. In situ TEM study showed that melting occurs between adjacent Ag nanoparticles at dimensions of between 15 and 40 nm at temperature of 400 °C [99]. In a related study when Ag nanoparticle sintering was treated as a liquid-state phenomena based on a Debye model with Lindemann's Law, the theoretical melting temperature was modelled as shown in Fig. 6 [50]. This model agreed with the experimental results which showed that nanoparticles will assume the melting temperature of bulk Ag properties at sizes larger than approximately 85 nm [50].

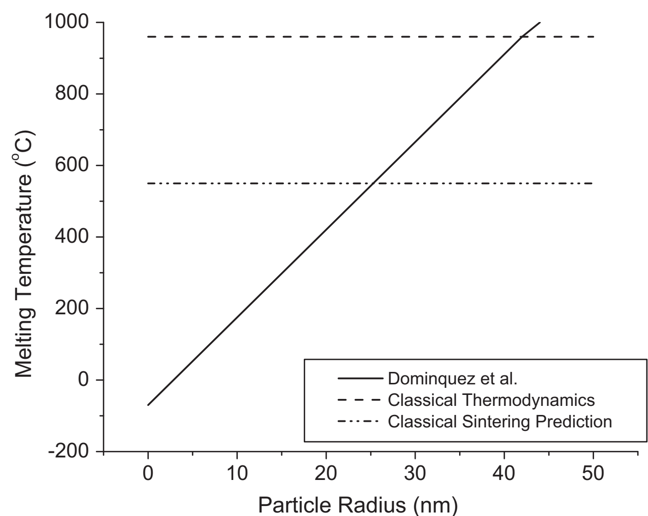

Fig. 6. Theoretical prediction of size-sintering relationships for Ag nanoparticles [50].
Reprinted with permission.

In pressureless sintering, van der Waals force also play a role in the adhesion of nanoscale Ag paste to the substrate at the nanometer scale [75]. Van der Waals forces attracted the Ag nanoparticles to the substrate which resulted in deformation and an increase of surface areas [75]. Based on the assumption of similar elements in nanoparticles and contacting surfaces, the van der Waals force (F_{vdW}) can be calculated with the following equation [73]:

$$F_{vdW} = -\frac{AR}{6D^2}$$

where A is the Hamaker constant (1×10^{-19} J); R is the nanoparticle radius (20×10^{-9} m); and D is the distance between the nanoparticle and the surface (0.2×10^{-9} m).

Based on the above typical values to simulate close contact, the van der Waals force comes to 8×10^{-9} N per nanoparticle. This force is quite sizable although this calculation has not taken the nanoparticle-to-nanoparticle interactions and the applied pressure from sintering into consideration. Additional surface area from this deformation increases the van der Waals force to attract more Ag nanoparticles to the surface for the sintering process [75].

In another study, applied pressures as low as 5 MPa were found to increase the shear strength as much as fourfold compared to pressureless sintering for a typical sintering temperature of 275 °C [68]. In this case, it is likely that “5 MPa” is the threshold stress for particle size of ~30 nm [68] although this can only be confirmed by the measurement of density in the sintered nano-Ag joint. The applied pressure for a nano-Ag joint is typically less than that used in sintering of micron-scale Ag particles which requires 10–40 MPa [6].

Threshold stress depends on the particle size because of the increasing contribution from the surface curvature of the particle as it becomes smaller as shown in Fig. 7 [100]. It is likely that there is a change of the diffusion mechanism to the more particle-size sensitive, diffusional creep, when sintering pressure is increased [101].

Besides the curvature of nanoparticles other processes which may contribute to the densification are stress-assisted diffusion, pore curvature driven diffusion and strain controlled pore closure, which have been reported for other nanoparticles [14]. However, such mechanistic study is lacking in the literature for Ag nanoparticles and deserves further attention.

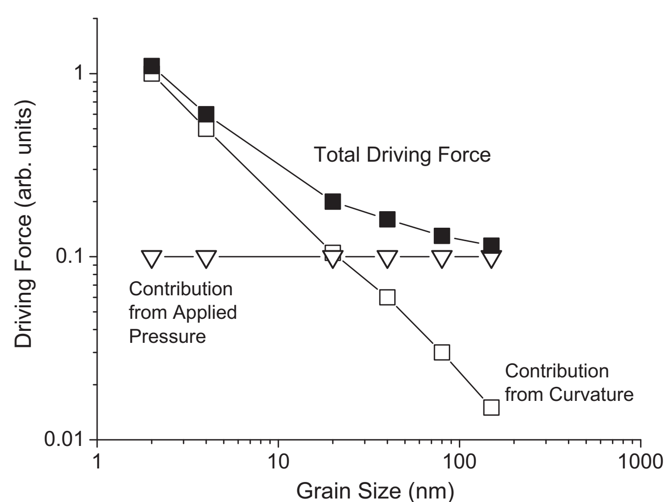

Fig. 7. Driving forces for nanopowder consolidation as a function of grain size [100] (reprinted with permission). *Note*: It should be noted that grain and particle size can be used interchangeably in Fig. 7 for the understanding of driving force to sintering although they do not refer to the same concept in the larger embodiment of literature. In general, there are two types of nanocrsytalline materials: single grains of nanometer size also known as ‘nanoparticles” or “crystallites” [14], or larger particles containing grain sizes of nanometer dimension.

4.3.2. Sintering temperature

As discussed earlier in Section 4.2.1 on “tensile strength”, an increase of sintering temperature will also increase the bonding strength because of increased decomposition of the dispersant which allows coalescence of Ag nanoparticles. Hence, the stability of dispersant plays a critical role in joint formation [45,56]. In one study, the bonding process of nano-Ag paste is modelled into two steps:

1. Detachment of dispersant which is related to the binding energies of functional groups facing the Ag surfaces (E_b).
2. Evaporation of the detached dispersant which is related to boiling point of the molecules forming the dispersant (E_v).

The total energy to remove the dispersants depends on the multiplicative sum of two factors ($E_b + E_v$) and the density of the molecules on the Ag surface (D) [56]. These factors were investigated experimentally with primary and secondary amines of different chain length as dispersants.

These researchers found that secondary amine-passivated Ag nanoparticles with shorter chain lengths produced higher die shear strength than with primary amine-passivated Ag nanoparticles in agreement with its quantum chemical prediction [56]. This quantum chemical calculation further postulated that dispersants with functional groups like thiol and carboxylic acids possess higher binding energies on Ag nanoparticles than those amine groups which would hamper their detachment during sintering [56]. However, comparison of shear strengths between carboxylate [35] and amine passivated [56] Ag nanoparticles from different researchers showed otherwise. This difference between theoretical and experimental results can be attributed to the higher sintering temperature of carboxylate-passivated Ag nanoparticles at 300 °C [35] versus 250 °C [56] for amine-passivated Ag nanoparticles of equal size.

4.3.3. Nanoparticle size, distribution and morphology

Besides the sintering temperature and pressure, effective sintering of Ag nanoparticles also depends on the particle size as shown in Fig. 8 for sintering at 300 °C [18,39,46]. As shown in Fig. 8, Ag nanoparticles of 11 nm have a shear strength six times larger than those produced from Ag particles of ~100 nm dimensions

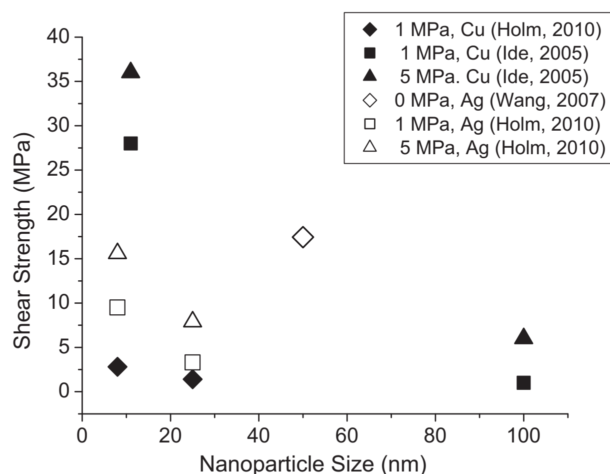

Fig. 8. Shear strength of Ag nanoparticles joints for bonding Ag or copper (Cu) substrates in ambient atmosphere for Ag nano-particle size ranging from 8 to 100 nm at sintering temperatures of 300 °C [18,39,46]. Holm et al. used Ag nano-ink in their work.

[46]. The reason was attributed to bonding interfaces: Ag particles (∼100 nm) were merely anchored without chemically bonding to the copper substrates. On the other hand, Ag nanoparticle joints (11 nm) fractured cohesively within the Ag joints instead of general adhesive failure at the Ag–Cu interface [46].

This trend is also supported by a study which showed that the densification rate of 30 nm Ag nanoparticles was substantially higher than those of 100 nm Ag nanoparticles [47]. The driving force for sintering can be significant for smaller diameter particles with greater curvature as discussed earlier in Fig. 7.

If the influence of sintering temperature is considered together with particle size the results may not be straightforward. In one study, room temperature sintering has been demonstrated with a shear strength of more than 8 MPa for diameters of Ag nanoparticles of 8 nm [84]. In another study Ag nanoparticles of 20 nm showed sintering behaviour at temperatures as low as 150 °C [48] although detectable bonding strength required sintering temperatures of 250 °C [32]. Others reported shear strengths of Ag joints exceeded the substrate strength when Ag nanoparticles of 50 nm were sintered at 160 °C for 30 min under pressure of 5 MPa [59]. There are many differences between these results including the sensitivity of the equipment to detect the bonding strength and testing configuration of the joints which overwhelm the influence of Ag nanoparticle size in the joint formation.

The measurement of grain (particle) size has also been a subject of controversy because of different methods (TEM versus XRD) and XRD protocols such as Scherrer and Warren Averbach used [7,102]. Good agreement can be found between these methods under certain circumstances like monodispersed and strain-free grain (particle) size. This important issue is often overlooked in published results and may hamper comparison between different researchers.

Besides particle size, other physical properties of Ag nanoparticles which influence the bonding properties are particle size distribution and particle morphology [31,103]. These factors affect the packing density of Ag nanoparticles which thereby affects the final density and strength of the nano-Ag joint. A larger distribution of particle sizes and different particle morphologies demonstrates better sintering properties which results in higher bonding strength [31]. Many researchers mixed micron-scale Ag particles with nano-Ag to produce denser joints [35,36,50,104]. In addition, micron-scale Ag particles have lesser amounts of dispersant and solvent associated with the lower surface-area-to-volume ratio compared to Ag nanoparticles.

In the context of particle morphology Ag nanorods (length ∼8 μm and diameters of 70 nm) produced joints with lower shear strengths than that of Ag nanoparticles [103]. The researchers did not postulate any possible reasons but it was likely to be caused by the inability of the nanorods to form a compact and dense joint.

4.3.4. Heating rate

Closely related to sintering temperature is the heating rate of the nanoscale Ag paste up to the final sintering temperature. A fast heating rate to a high sintering temperature promoted a dense structure [39]. It should be mentioned here that surface diffusion is the dominant mechanism for low temperature sintering while grain boundary or lattice diffusion dominates the high temperature sintering of nanopowders [14]. A high heating rate minimized aggregation of nanoparticles during the ramp-up to the high sintering temperature [68]. When nanoparticles aggregated or agglomerated into a larger effective radius, higher sintering temperatures were required to reach the equivalent higher relative density [105]. The latter example is based on titania nanoparticles but the same principle is expected to govern the sintering mechanism of Ag nanoparticles. Unlike sintering of bulk ceramics, Ag nanoparticles did not face the issue of low heat transfer during high heating rate because of its high thermal conductivity which heated the entire printed/dispensed area almost instantaneously (phonon-limited transfer).

On the other hand, the heating rate should be low enough to allow the adequate outgassing of the solvent without disrupting the bond line thickness of the nanoscale Ag paste. A rate of ∼10–20 °C/min appears to be the optimum heating rate for some researchers [39] although others have used higher heating rates of 60 °C/min [46]. The latter investigation imposed a constant pressure of 1–5 MPa during the bonding process to ensure the outgassing solvent did not lift the dies during sintering [46]. In a mixture of Ag micron-sized and nanoparticles, liquefaction of Ag nanoparticles was observed near the contact areas of adjacent particles when the heating rate was carried out at 10 °C/min [50]. Such thermal transition stress induced macroscopic cracks [50] which could delaminate the nano-Ag from the surfaces.

Another approach to reduce the heating rate for sintering is to introduce a separate drying profile, e.g. sequentially higher temperatures of 50 °C, 100 °C and 180 °C, before the sintering step [106]. In the case of large bonding areas, e.g. 25 mm^2, a double-print process was used which involved an interim step of drying the nanoscale Ag paste before applying a second layer of nanoscale Ag paste before final steps of die attaching [106]. This variation in process steps would ensure complete outgassing of the solvents from the paste which might otherwise disrupt the sintering process.

4.3.5. Dimension of bonding area

Besides the heating rate, the bonding area dimensions also influenced the nano-Ag joint shear strength. Using a die-shear configuration, it was reported that the shear strength decreased as much as 30% for an increase of bonding area from 3.9 mm^2 to 5.4 mm^2 [107]. There is an increased risk of solvents unable to escape from inner areas of the bonding interfaces with an increase of bonding area. Subsequent sintering temperature, which is typically higher than the preheating temperature, will cause violent outgassing which interferes with the sintering process. Oxygen takes a longer diffusion path to inner die area to oxidize the dispersant. Such lack of sintering at centre of the bonding areas has been reported elsewhere [18].

Microstructure studies of sintered nano-Ag joints also supported these proposed mechanisms [95]. An air-sintered nanoscale Ag paste under a chip looked similar to the surface of an exposed nano-Ag sintered under a nitrogen environment [95]. This discussion on “out-diffusion of solvent and in-diffusion of oxygen” suggests that the thickness of the nanoscale Ag paste in the manufacture of the bond is also likely to play a role in controlling the strength of the joints though this factor is not actively researched in the literature. The main reason for lack of interest in this area because die attach thickness is governed by other electrical and thermal conductivity consideration.

As mentioned earlier oxygen is needed during sintering of nanoscale Ag paste to fully oxidize the dispersant derived from fatty acids on the Ag nanoparticles [35,45,46]. Hence, it is expected that nano-Ag joints produced in an ambient environment possess consistently higher strength than those produced in a nitrogen atmosphere.

4.3.6. Bonding substrate

The foregoing discussion has been primarily dealing with intraparticle cohesion via various mechanisms of sintering. An equally important aspect to determine the strength of the joint is the adhesion strength of the Ag nanoparticles on the bonding substrate surface. One group of researchers demonstrated that the ambient environment sintering of nanoscale Ag paste produced lower die shear strength than those sintered in a nitrogen atmosphere [35]. They attributed this result to the oxidation of the copper substrate.

Others reported that this oxidized copper layer did not interfere in the formation of Cu–Ag inter-diffusion layer which is the key to a strong joint [75]. A partial oxygen pressure of 0.08 atm was considered optimum to oxidize the dispersant while preventing excessive oxidation of the copper substrate [108].

As demonstrated in Figs. 4, 5, 8 and 9, Ag nanoparticles have been successfully used as bonding materials on different surfaces like Au-plated copper, Ag plated with and without nickel diffusion barrier plating, and bare copper. As expected, nano-Ag paste bonds easily on Ag-plated substrate because the chemistry is the same across the interface, and the lattice constant is similar between substrate and paste. Due to similar atoms between paste and substrate, it is not possible to track the diffusion of Ag atoms from Ag paste into the Ag plated substrate.

In the case of a sputtered Au coating the diffusion distance of Au into Ag joint reached a distance of 300 nm [37]. The oxidation-free surfaces and comparable lattice constants of Au and Ag eased the bonding process with Ag nanoparticles [32]. The crystal orientation of Ag atoms and Au atoms suggested quasi-epitaxial growth of Ag on the Au substrate [32,109]; silver and gold are completely miscible couple. Epitaxial growth will reduce the overall energy of this bonding process. Others reported that higher sintering temperatures are required for bonding on Au-plated substrates to achieve a comparable strength to a Ag plated substrate [110]. A likely reason is the need to have additional energy, i.e. thermal energy, to overcome the higher activation energy for inter-diffusion of Ag atoms in dissimilar materials.

Good bonding results for copper substrate were generally aided by the surface preparation methods which removed copper oxides from the substrate with diluted nitric acid [84] or hydrochloric acid [37,38,46,63] prior to applying nanoscale Ag paste. The thickness of naturally occurring copper oxides varied from 23 to 147 nm [111]. There were also some speculations that the decomposition of the dispersant deoxidized the oxide film on the copper surfaces for the bonding process [37,38,46].

Compared with a Au plated substrate, the Cu–Ag diffusion layer from Ag nanoparticles, on the copper substrate lacked the epitaxial formation in Ag–Au surfaces because of difference in lattice constants and electrochemical differences; copper (0.3615 nm), gold (0.4079 nm) and Ag (0.4086 nm) [32]. The percentage of diffusing copper in Ag joints were found to be less than 4 weight percent at 10 nm from the Ag–Cu interface [32]. Other researchers showed that these Ag nanoparticles wet the Cu substrate and form epitaxially oriented islands by grain boundary migration upon annealing at 100 °C [112]. A contrast belt of less than one nm was also reported in the bonding interface of Ag–Cu substrate [58]. These observations suggested that a metallic bond was formed between silver atoms on copper substrates despite the lattice mismatch between Cu and Ag [58]. These researchers attributed the differences in interfacial properties to the thickness and composition of dispersant [58]. There was also some success reported for bonding of nano-Ag with bare nickel as a joining substrate [37]. Less success was reported for the bonding of nanoscale Ag paste on aluminium and titanium because of their stable surface oxides which could not be reduced by decomposition of the dispersants on Ag nanoparticles [37]. The shear strength results of nano-Ag bonding with nickel substrates were better than those of Al and Ti, but only ~50% of the copper substrate bonding strength [37].

Amongst the different substrates, bonding on copper substrate is likely to be gaining more interest in the future because many electronic packaging schemes tend to favour bare copper leadframe over Ag plated leadframe. Consistent bonding results on copper substrate are still lacking but one notable approach reported in literature will be exploiting on the decomposition of organic Ag compounds like Ag_2CO_3 to bond on copper surfaces [76]

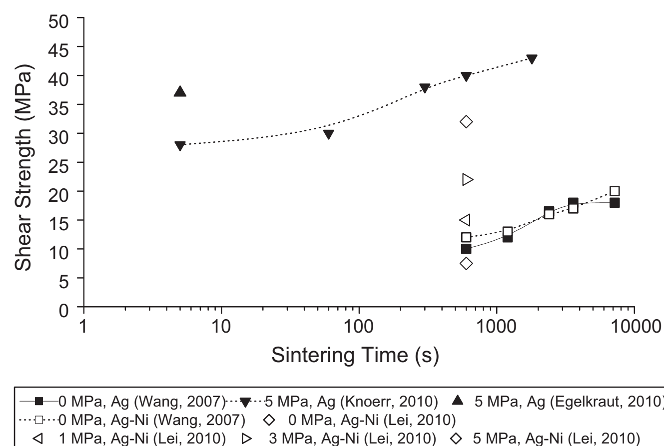

Fig. 9. Shear strength of Ag nanoparticles joints for bonding Ag plated substrates for different sintering time in ambient atmosphere for Ag nano-particle size between 30 and 50 nm at sintering temperatures between 275 °C and 285 °C [39,68,95,113]. "Ni" refers to a diffusion barrier nickel plating layer on the copper substrate before plating Ag layer.

4.3.7. *Sintering time*

Another factor which strongly influenced the shear strength is the sintering time. Based on Fig. 9, an increase of sintering time leads to an increase in shear strength regardless of the joint design [39,68,95,113]. The mechanism is likely to be similar to an increase of sintering temperature which exposes more unpassivated Ag nanoparticles for sintering with adjacent nanoparticles with an increase in time. Sintering is a diffusion-controlled mechanism which depends on time for progress. In the presence of applied pressure as shown in Fig. 9, the trend of increasing shear strength with increase of sintering time remains but the absolute values of those with pressure are higher than those without pressure. Applied pressure increases the number of contact surfaces between adjacent Ag nanoparticles to form strong bond.

The influence of sintering time must also be taken together within the context of the targeted sintering temperature. At higher sintering temperatures the densifying mechanisms like grain boundary and lattice diffusion will be operating to densify the nano-Ag joint [47]. If the sintering temperature is too low, further heating will only result in grain growth instead of densification which naturally leads to lower shear strength.

However, the optimum duration of sintering varies between different nanoscale Ag pastes and joint design. In one study, the optimum shear strength of 17–18 MPa was reported after 60 min of sintering time [39]. Using similar nanoscale Ag pastes, an increase of 30% in shear strength to 40 MPa was measured when the sintering time was increased from 5 to 60 s [95]. During this period the density of the nano-Ag joint increased from 68% to 75%. By comparison, the initial 5 s of sintering was sufficient to increase the density from 45% to 68% with a corresponding increase of shear strength from 23 MPa to 30 MPa [95]. This rapid sintering within the first few seconds suggested that the coalescence of Ag nanoparticles occurred as soon as the dispersants were oxidized under heat and pressure [95]. This fast sintering has also been predicted by Monte Carlo simulation methods with tight binding many-body potentials for sintering of two Ag nanoparticles [58].

Even short duration heating of less than a minute during testing was also found to increase the tensile strength of the nano-Ag joint because of continuing coalescence of Ag nanoparticles to neighbouring Ag nanoparticles [58]. In prolonged sintering times, the concentration of crystal defects was reduced and the macroscopic flow of materials increased the nano-Ag density [39].

High temperature storage testing of sintered nano-Ag joints with Ni–Ag plated substrate at 200 °C also resulted in an increase of shear strength up to 500 h [113]. When these nano-Ag joints were stored for another 500 h at 200 °C, the shear strength remained stable. The researchers speculated on several possibilities including the diffusion of the nickel layer into the porous Ag layer to reduce any further increase of shear strength with prolonged ageing time [113].

In their report, the microstructure of nano-Ag joint showed coarser structure and larger pores with increasing ageing time [113]. The authors did not comment on the ratio of "annular flaw size/pore radius" but annealing at 200 °C could reduce this ratio to improve the mechanical properties. A likely mechanism is surface diffusion which has been reported to be the dominant mass transport mechanism for grain growth in sputter-deposited nanocrystalline Ag [114]. Such an annealing approach has been carried out on compacted nanocrystalline copper albeit at a lower temperature of 150 °C for nine hours to improve its mechanical properties [115].

An important aspect which is seldom mentioned in the nano-Ag joint is the grain growth during sintering. Compacted Ag nanoparticles of different density from 85 to 95% exhibited abnormal grain growth at 190–210 °C when investigated by dynamic heating methods such as DSC [86]. High temperature annealing studies of 30 min put the grain growth temperature for this compacted Ag nanoparticles (density of 97%) at 150 °C [30]. The range of densities were slightly higher than those reported for sintered nano-Ag joint at 85–90% density [95]. Examination of sintered nano-Ag joints did not reveal any well-delineated grain size. It is likely that the porosity played a critical role in preventing any grain growth for this sintered nano-Ag.

Inherently the joints made from Ag nanoparticles are more stable than lead-free or Sn–Pb solder because the former assumes the thermal stability of Ag which has a low homologous temperature of 0.3. This thermal stability was also demonstrated by a stable electrical resistivity when operating at above 500 °C [15].

4.4. Thermal fatigue properties

In the public literature, there are some limited thermal cycling results of microelectronic packages produced with Ag nanoparticles as the die bonding materials [35,36,85,116]. These limited studies demonstrated the ability of nano-Ag joint to operate in thermal cycling application, often multiple times better than typically processed Sn–Pb solder joint. The following paragraphs describe these experiments in greater details and different factors influencing its performance in thermal cycling environment.

In one study, nano-Ag joints with passive dies passed 800 cycles of temperature cycling (TC) (−40 to 125 °C) without any significant changes in the microstructure and/or cracks [85]. The researchers attributed these good mechanical properties to the plastic deformation of the porous sintered Ag nanoparticles which absorbed the thermal stresses. Although porosity is not mentioned as contributing factor by the author [85], pores are known to minimize grain growth which is detrimental to the mechanical properties of nanomaterials [101]. However, it should be mentioned that this experiment used a less stringent temperature cycling test compared to those described in the following TC test (−55 °C to 175 °C).

In separate study with similar nanoscale Ag paste but with different processing parameters, sintered nano-Ag joints proved to be more reliable than Sn–Ag–Cu alloy and Pb–5Sn alloy in thermal and power cycling tests [116]. These researchers attributed the good property of sintered joints to the high density, high joint strength and high elastic strain which led to slower failure as per the Coffin–Mason law. According to this model and Suhir's, the lifetime of Ag sintered joints was 4000× longer than typical solder joints.

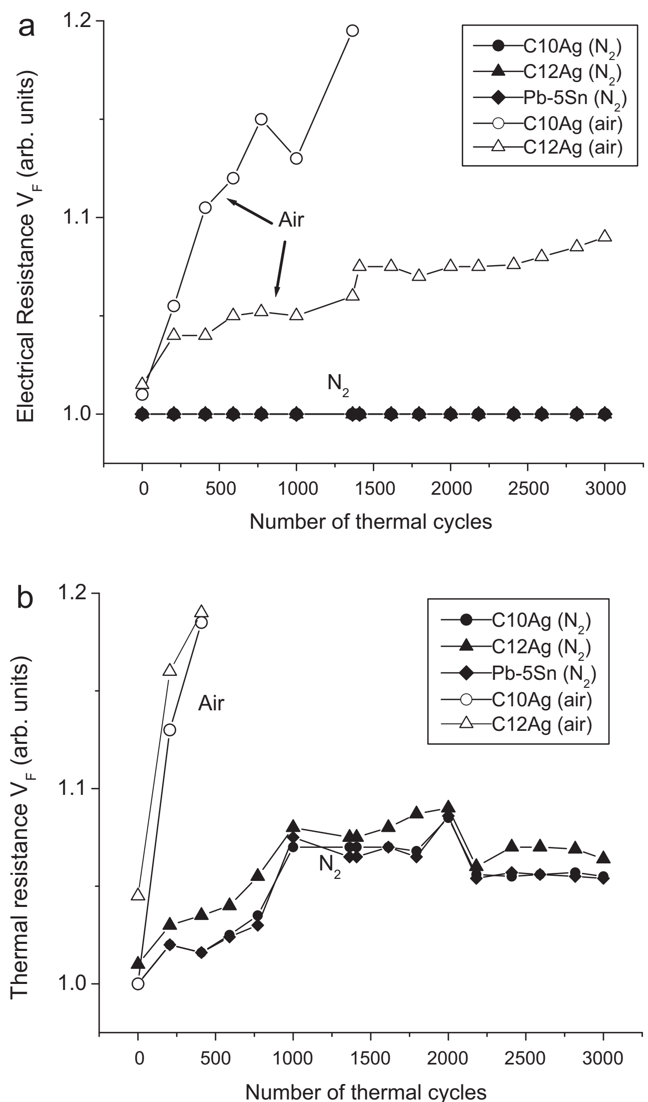

Fig. 10. Graphs of (a) electrical resistances VF (b) thermal resistances VF of diode packages made from each paste. Circles: C10Ag paste. Triangles: C12Ag. Open: sintered in air. Solid: sintered in N_2. Diamonds: high temperature Pb–5Sn solder paste. The values for VF and ΔVF are normalized by thermal resistance for Pb–5Sn solder at zero thermal cycle [35].

Reprinted with permission.

In another Ag sintered nano-joint study with live devices as shown in Fig. 10, there was no changes in the electrical resistance (V_F) for joints sintered in N_2 after 3000 cycles [35]. Air-sintered nano-Ag joints appeared to be less reliable with a sharper increase in thermal and electrical resistance for joints made from C10Ag but a more moderate increase in the C12Ag paste. It was suggested that the beneficial effect of sintering in air which involved rapid oxidation of dispersant was offset by oxidation of the copper substrate. Another possible reason which was not raised in the paper is the composition of the Ag paste. C10Ag andC12Ag had weight percentages of 84% and 60% of 0.4 μm-scale Ag particles. The beneficial effect of sintering in air may not be substantial because of the high percentages of micron-scale Ag particles in these pastes.

4.5. Recent innovations in LTJT

In recent times, there are many innovations in LTJT to improve the adoption by industry such as in the area of applying the nano-Ag on designated area and the materials properties.

In the area of applying Ag nanoparticles in the joint area, there are some recent innovations. Similar to reactive inkjet printing, Ag nanoparticles can be formed in situ in the joining area by the reduction of Ag_2O with triethylene glycol at a decomposition temperature between 130 °C and 160 °C [89]. These newly formed Ag nanoparticles sintered and the joint strength improved to ∼60 MPa when further heated up to 250 °C [89]. In reactive inkjet printing, $AgNO_3$ and reducing agents like ascorbic acid are printed consecutively for in situ formation of Ag nanoparticles to build an interconnect structure [117]. Such approaches provide another route for forming nano-Ag joints without resorting to printing or dispensing of nanoscale Ag pastes. In the absence of heat used to form the Ag joints, dispersants like dodecylamine could be removed by methanol to affect the coalescence of Ag nanoparticles [84,118].

In another approach, Ag nanoparticles are precipitated on the joint area via vaporization and condensation in a precipitation chamber filled with helium [119]. Then, these nanoparticles were pre-sintered at 120–350 °C before bonding at 9 MPa and 180–250 °C. Some processing details may be missing from this disclosure because self-coalescence would increase the Ag nanoparticle size to the micron range in the absence of a passivation step which would surely increase the sintering temperature to more than 250 °C.

In the area of materials development different core–shell alloys like Cu–Ag [120] or Ni–Ag are used to form the nano-Ag joint instead of pure Ag nanoparticles [34]. This approach is expected to further improve the mechanical and electrical properties of the joints. A similar objective could be achieved by mixing copper particles, as much as 2700 ppm, into nanoscale Ag pastes [31]. Copper nanoparticles improved the bondability of nano-scale Ag paste to copper surfaces by forming a nanostructural solute solution [38].

Others added diamond particles into the Ag nanoparticles to better match the coefficient of thermal expansion (CTE) with silicon die and improve the thermal conductivities [28,121]. Silicon carbide particles were also added to the nanoscale Ag paste for the same reason [28,122]. The linear CTEs of silicon, silicon carbide and diamonds at 20 °C are 3.0, 4.4 and 1.0 (10^{-6}/°C), respectively [123,124]. In the presence of these different nanoscale materials, different intermolecular forces like van der Waals, electrostatic, steric, etc., are expected to play a role in the formulation of the paste and eventually affecting the mechanical properties of the joints. Although unlikely to happen attention should be paid to any detrimental phase transformations which might occur within the operating temperature range to reduce the good thermal or physical properties of these additives.

4.6. Future challenges in LTJT

LTJT using nano-Ag has achieved great strides in the materials formulation and application but wide spread adoption of this technology is likely to face environmental challenges. Nano-Ag is toxic to many micro-organisms including those which are ecologically relevant species [125]. The use of Ag nanoparticles will be severely curtailed if these studies show that they are indeed detrimental to the environment [126].

The commercialization of nano-Ag as LTJT material also faces the challenges of escalating price of Ag flakes and powders because suppliers typically include the Ag base metal price as part of their costing. This trend prompts the development of mixed nanoparticles like Cu–Ag to reduce the percentage of Ag loading [38] or mixing with micron-scale Ag particles which cost only one tenth of Ag nanoparticles [35,36,50,104] or alloying with other elements. The alloying approach has the added advantage of reducing silver migration reported in the literature recently [90,127]. The literature on these mixed Ag particles is less widely available. Although these initial studies on mixed Ag particles are encouraging, more confirmatory work is needed to fully understand the sintering mechanism and formation of additional phases for mixed elements which may occur under an applied pressure.

Even in the pure Ag nanoparticle, there is still some knowledge gaps in the area of mechanical properties of nano-Ag joint such as thermal fatigue properties with only four studies found by the author in the literature. Theoretical understanding of microstructural evolution (such as coarsening and closure of porosity) during formation of nano-Ag joint is somewhat lacking though they are expected to be the same as sinter forging of other metallic nanoparticles. These densification mechanisms are different from pressureless sintering. Currently, most studies are directed at demonstrating the feasibility of using nano-Ag as interconnect materials, as opposed to the long-term behaviours in the field.

Another challenge facing the nano-Ag is the lack of production equipment which can demonstrate the good properties of nano-Ag as bonding materials without compromising the production throughput. Company like Semikron developed bonding equipment for their internal use to bond component [128]. Other equipment manufacturers have jumped into bandwagon by filing patents in this area [42] but commercial prototypes are lacking. Most microelectronic packaging companies are relatively new to sintering technology and hence, their reluctance to invest in new technology without definite return of investment.

5. Conclusions

In conclusion, this review discusses at length, the various factors which influence the formation of nano-Ag joints such as sintering pressure, sintering temperature, sintering time, sintering environment, heating rate, type of substrates and physical properties of Ag nanoparticles like sizes, particle size distribution and morphology. The purpose of this discussion is to demonstrate the bulk of knowledge in this area and its close relationship to the field of processing and using ceramic and metallic nano-powders albeit in unconstrained manner for the latter.

LTJT using Ag paste has a long history of development and implementation since the late 1980s. While long term mechanical properties of joints made from micron-scale Ag are acknowledged and widely available, the same cannot be said for the die attach joints made from Ag nanoparticles. Besides the knowledge gap in this area, LTJT using nano-Ag needs to overcome several hurdles such as environmental challenges, escalating silver price and wider availability of production-type die bonding equipment. Nevertheless, this area of research is currently attracting the best brains of microelectronic industry to solve these issues with new bonding concepts and materials composition.

Acknowledgements

The author would like to express his heartfelt gratitude to his colleagues, relatives, friends, suppliers and reviewers of this journal for suggestions, discussions and help rendered throughout the publication of this review. Special thanks to J. Parsey (On Semiconductor), Lam Y.M. (NTU) and Chen Z. (NTU) for critically reviewing this paper. The author would also to thank his managers at On Semiconductor, Shutesh Krishnan and C.H. Chew, for supporting his work.

References

[1] K. Suganuma, S.J. Kim, K.S. Kim, JOM 61 (2009) 64–71.
[2] Y. Takaku, I. Ohnuma, Y. Yantada, Y. Yagi, I. Nakagawa, T. Atsumi, M. Shirai, K. Ishida, ASTM Spec. Tech. Publ. 1530 (2011) 27–49.
[3] V. Chidambaram, J. Hattel, J. Hald, Microelectron. Eng 88 (2011) 981–989.

[4] C. Buttay, D. Planson, B. Allard, D. Bergogne, P. Bevilacqua, C. Joubert, M. Lazar, C. Martin, H. Morel, D. Tournier, C. Raynaud, Mater. Sci. Eng. B: Solid-State Mater. Adv. Tech. 176 (2011) 283–288.
[5] R. Sharp, IEEE Colloq. (Dig.) (1999) 1–4.
[6] H. Schwarzbauer, R. Kuhnert, IEEE Trans. Ind. Appl. 27 (1991) 93–95.
[7] J.R. Groza, in: C.C. Koch (Ed.), Nanostructured Materials: Processing, Properties and Potential Applications, Noyes Publication, Norwich, 2002.
[8] X. Cao, T. Wang, K.D.T. Ngo, G.Q. Lu, IEEE Trans. Compon. Pack. Manuf. Tech. 1 (2011) 495–501.
[9] H.S. Chin, K.Y. Cheong, A.B. Ismail, Metal. Mater. Trans. B 41 (2010) 824–832.
[10] V.R. Manikam, K.Y. Cheong, IEEE Trans. Compon. Packag. Manuf. Tech. 1 (2011) 457–478.
[11] R. Kisiel, Z. Szczepaenski, Microelectron. Rel. 49 (2009) 627–629.
[12] G. Palm, US2005/0247760A1, Semikron Elektronik GmbH, 2005.
[13] H. Schwarzbauer, US4810672, Siemens AG, 1989.
[14] M.J. Mayo, Int. Mater. Rev. 41 (1996) 85–115.
[15] J.G. Bai, Z.Z. Zhang, J.N. Calata, G.Q. Lu, IEEE Trans. Compon. Packag. Tech. 29 (2006) 589–593.
[16] G. Bai, Low-temperature Sintering of Nanoscale Silver Paste for Semiconductor Device Interconnection, PhD thesis, Virginia Polytechnic Institute and State University Blacksburg, Virginia, 2005.
[17] Z. Wei, M. Zhou, H. Qiao, L. Zhu, H. Yang, T. Xia, J. Nanomater 968058 (2009) 1–5.
[18] E.A. Holm, J.D. Puskar, M. Reece, V. Tikare, G.C. Cardona, L.N. Brewer, Nanocrystal Enabled Solid State Bonding SAND2010-7013, Sandia National Laboratories, 2010, 31.
[19] R. Kuhnert, H. Schwarzbauer, US5379942, Siemens AG, 1995.
[20] W. Knapp, USA, US6935556B2, ABB Research Ltd, 2005.
[21] H. Schwarzbauer, US4903885, Siemens AG, 1990.
[22] H. Schwarzbauer, US5058796, Siemens AG, 1991.
[23] H. Schwarzbauer, US5169804, Siemens AG, 1992.
[24] E. Ide, T. Morita, Y. Yasuda, US2010/0195292A1, Hitachi Ltd, 2010.
[25] I.J. Rasiah, US7083850B2, Honeywell International Inc., 2006.
[26] R. Kajiwara, S. Motowaki, K. Ito, T. Ishii, K. Arai, T. Nakajo, H. Kagii, US2010/0195292A1, Renesas Technology Corp, 2010.
[27] W. Baumgartner, J. Fellinger, US4856185, Siemens AG, 1989.
[28] H. Schwarzbauer, US6823915B2, Siemens AG, 2004.
[29] C.A. Lu, P. Lin, H.C. Lin, S.F. Wang, Jpn J. Appl. Phys. Part 1: Regul. Pap. Short Notes Rev. Pap. 45 (2006) 6987–6992.
[30] N.P. Kobelev, Y.M. Soifer, R.A. Andrievski, B. Gunther, Nanostructur. Mater. 2 (1993) 537–544.
[31] C. Fruh, M. Gunther, M. Rittner, A. Fix, M. Nowottnick, Proc. 2010 Electron. Syst. Integr. Tech. Conf., 2010, pp. 1–5.
[32] Y. Akada, H. Tatsumi, T. Yamaguchi, A. Hirose, T. Morita, E. Ide, Mater. Trans. 49 (2008) 1537–1545.
[33] M. Boureghda, N. Desai, A. Lifton, O. Khaselev, M.T. Marczi, B. Singh, US2009/0025967A1, Fry's Metal Inc., 2009.
[34] H. Hozoji, T. Morita, H. Sasaki, US7393771B2, Hitachi Ltd, 2008.
[35] H. Ogura, M. Maruyama, R. Matsubayashi, T. Ogawa, S. Nakamura, T. Komatsu, H. Nagasawa, A. Ichimura, S. Isoda, J. Electron. Mater. 39 (2010) 1233–1240.
[36] M. Maruyama, R. Matsubayashi, H. Iwakuro, S. Isoda, T. Komatsu, Appl. Phys. A: Mater. Sci. Process 93 (2008) 467–470.
[37] E. Ide, S. Angata, A. Hirose, K.F. Kobayashi, Mater. Sci. Forum 512 (2006) 383–388.
[38] Y. Morisada, T. Nagaoka, M. Fukusumi, Y. Kashiwagi, M. Yamamoto, M. Nakamoto, J. Electron. Mater. 39 (2010) 1283–1288.
[39] T. Wang, X. Chen, G.Q. Lu, G. Lei, J. Electron. Mater. 36 (2007) 1333–1340.
[40] M. Tobita, Y. Yasuda, US2009/0180914A1, Hitachi Ltd, 2009.
[41] W. Schmitt, M. Schafer, H.W. Hagedorn, US2010/0051319A1, W.C. Heraeus GmbH 2010.
[42] T. Maeda, US7726546B2, Shinkawa Ltd, 2010.
[43] Y. Yato, T. Nakajo, H. Oka, US2009/0189264A1, Renesas Technology Corp, 2009.
[44] C. Mertens, J. Rudzki, R. Sittig, IEEE Ann. Power Electron. Special. Conf. 6 (2004) 4178–4182.
[45] M. Knoerr, A. Schletz, S. Oertel, M. Jank, Proc. 6th World Congress Part. Tech. 4S (2010) 1–4.
[46] E. Ide, S. Angata, A. Hirose, K.F. Kobayashi, Acta Mater. 53 (2005) 2385–2393.
[47] G. Bai, G. Lei, J. Calata, G.Q. Lu, J. Mater. Res. 22 (2007) 3494–3500.
[48] K.S. Moon, H. Dong, R. Maric, S. Pothukuchi, A. Hunt, L. Yi, C.P. Wong, J. Electron. Mater. 34 (2005) 168–175.
[49] K. Lu, Int. Mater. Rev. 53 (2008) 21–38.
[50] N.B. Bell, C.B. DiAntonio, D.B. Dimos, J. Mater. Res. 17 (2002) 2423–2432.
[51] H. Zhu, R.S. Averback, Philos. Mag. Lett. 73 (1996) 27–33.
[52] G. Frens, J.T.G. Overbeek, Colloid Poly. Sci. 233 (1969) 922–929.
[53] A.R. Tao, S. Habas, P. Yang, Small 4 (2008) 310–325.
[54] B.L. Cushing, V.L. Kolesnichenko, C.J. O'Connor, Chem. Rev. 104 (2004) 3893–3946.
[55] Y.A. Krutyakov, A.A. Kudrinskiy, A.Y. Olenin, G.V. Lisichkin, Russ. Chem. Rev. 77 (2008) 233–257.
[56] M. Tobita, Y. Yasuda, E. Ide, J. Ushio, T. Morita, J. Nanopart. Res. 12 (2010) 2135–2144.
[57] K. Park, D. Seo, J. Lee, Coll. Surf. A: Physicochem. Eng. Aspects 313–314 (2008) 351–354.
[58] A. Hu, J.Y. Guo, H. Alarifi, G. Patane, Y. Zhou, G. Compagnini, C.X. Xu, Appl. Phys. Lett. 97 (2010) 1531171–1531173.
[59] H. Alarifi, A. Hu, M. Yavuz, Y.N. Zhou, J. Electron. Mater. 40 (2011) 1394–1402.
[60] D. Jiang, J. Xie, M. Chen, D. Li, J. Zhu, H. Qin, J. Alloys Compd. 509 (2011) 1975–1979.
[61] X. Wang, Y. Lin, F. Gu, Z. Liang, X.F. Ding, J. Alloys Compd. 509 (2011) 7515–7518.
[62] J. Liu, X. Li, X. Zeng, J. Alloys Compd. 494 (2010) 84–87.
[63] H. Nagasawa, M. Maruyama, T. Komatsu, S. Isoda, T. Kobayashi, Phys. Status Solidi (A) Appl. Res. 191 (2002) 67–76.
[64] M. Yamamoto, M. Nakamoto, J. Mater. Chem. 13 (2003) 2064–2065.
[65] M. Yamamoto, Y. Kashiwagi, M. Nakamoto, Langmuir 22 (2006) 8581–8586.
[66] D. Wakuda, M. Hatamura, K. Suganuma, Chem. Phys. Lett. 441 (2007) 305–308.
[67] G.Q. Lu, G. Lei, J.N. Calata, WO2009/094537A2, Virginia Tech Intellectual Properties Inc., 2009.
[68] T.G. Lei, J.N. Calata, G.Q. Lu, X. Chen, S. Luo, IEEE Trans. Compon. Package Tech. 33 (2010) 98–104.
[69] L.H. Liang, C.M. Shen, S.X. Du, W.M. Liu, X.C. Xie, H.J. Gao, Phys. Rev. B Condens. Matter Mater. Phys. 70 (2004) 2054191–2054195.
[70] V. Keith, M.G. Ward, Cryogenics 24 (1984) 249–250.
[71] M. Grouchko, I. Popov, V. Uvarov, S. Magdassi, A. Kamyshny, Langmuir 25 (2009) 2501–2503.
[72] S. Magdassi, M. Grouchko, O. Berezin, A. Kamyshny, ACS Nano 4 (2010) 1943–1948.
[73] J. Israelachvili, Intermolecular and Surface Forces, 3rd ed., Elsevier, Burlington, 2011.
[74] J. Perelaer, P.J. Smith, D. Mager, D. Soltman, S.K. Volkman, V. Subramanian, J.G. Korvink, U.S. Schubert, J. Mater. Chem. 20 (2010) 8446–8453.
[75] S. Joo, D.F. Baldwin, Nanotech 21 (2010) 055204–055215.
[76] W. Schmitt, T. Dickel, K. Stenger, US2009/0134206A1, W.C. Heraeus GmbH, 2009.
[77] K.H. Tseng, C.Y. Liao, D.C. Tien, J. Alloys Compd. 493 (2010) 438–440.
[78] D. Yu, X. Chen, G. Chen, G. Lu, Z. Wang, Mater. Des. 30 (2009) 4574–4579.
[79] X. Chen, R. Li, K. Qi, G.Q. Lu, J. Electron. Mater. 37 (2008) 1574–1579.
[80] J.R. Greer, R.A. Street, J. Appl. Phys. 101 (2007) 1035291–1035295.
[81] A.V. Panin, A.R. Shugurov, K.V. Oskomov, Phys. Solid State 47 (2005) 2055–2059.
[82] R.W. Hertzberg, Deformation and Fracture Mechanics of Engineering Materials, 4th ed., John Wiley & Sons Inc, New York, 1996.
[83] V. Krstic, U. Erb, G. Palumbo, Scr. Metall. Mater. 29 (1993) 1501–1504.
[84] D. Wakuda, K.-S. Kim, K. Suganuma, IEEE Trans. Compon. Package Tech. 33 (2010) 437–442.
[85] J. Li, Thermo-mechanical reliability of sintered silver joint versus lead-free solder for attaching large area devices, MSc thesis, Virginia Polytechnic Institute and State University, Blacksburg, Virginia, 2010.
[86] A. Kumpmann, B. Guenther, H.D. Kunze, Mater. Sci. Eng. A 168 (1993) 165–169.
[87] Y.W. Cheng, T.A. Siewert, J. Electron. Mater. 32 (2003) 535–540.
[88] M.H. Sloboda, Weld. Metal Fabr. 29 (1961) 291–296.
[89] A. Hirose, H. Tatsumi, N. Takeda, Y. Akada, T. Ogura, E. Ide, T. Morita, J. Phys. Conf. Ser. 165 (2009) 012074–012079.
[90] Y. Mei, G.Q. Lu, X. Chen, S. Luo, D. Ibitayo, IEEE Trans. Device Mater. Rel. 11 (2011) 316–322.
[91] I. Nakamori, H. Nakamura, T. Hayano, S. Kagawa, Bull. Chem. Soc. Jpn. 47 (1974) 1827–1832.
[92] Y. Chiu, U. Rambabu, M.H. Hsu, H.P.D. Shieh, C.Y. Chen, H.H. Lin, J. Appl. Phys. 94 (2003) 1996–2001.
[93] G.I.N. Waterhouse, G.A. Bowmaker, J.B. Metson, Phys. Chem. Chem. Phys. 3 (2001) 3838–3845.
[94] B.V. L'Vov, Thermochim. Acta 333 (1999) 13–19.
[95] M. Knoerr, A. Schletz, Proc. 6th Int. Conf. Integr. Power Electron. Syst., 2010, pp. 1–6.
[96] R.B. Schwarz, P.B. Desch, S. Srinivasan, P. Nash, Nanostructur. Mater. 1 (1992) 37–42.
[97] S.J. Zhao, S.Q. Wang, D.Y. Cheng, H.Q. Ye, J. Phys. Chem. B 105 (2001) 12857–12860.
[98] F. Baletto, R. Ferrando, Rev. Mod. Phys. 77 (2005) 371–423.
[99] T. Yonezawa, Biomed. Mater. Eng. 19 (2009) 29–34.
[100] G. Skandan, Nanostruct. Mater. 5 (1995) 111–126.
[101] J.R. Groza, R.J. Dowding, Nanostruct. Mater. 7 (1996) 749–768.
[102] K.S. Siow, A.A.O. Tay, P. Oruganti, Mater. Sci. Tech. 20 (2004) 285–294.
[103] J. Jiu, K. Murai, K. Kim, K. Suganuma, Proc. 7th IEEE Conf. Polym. Adhes. Microelectron. Photonics, 2008, pp. 1–5.
[104] K. Suganuma, S. Sakamoto, N. Kagami, D. Wakuda, K.S. Kim, M. Nogi, Microelectron. Rel. (2011), doi:10.1016/j.microrel.2011.1007.1088.
[105] M.J. Mayo, D.C. Hague, D. Chen, Mater. Sci. Eng. A 166 (1993) 145–159.
[106] X. Cao, T. Wang, Z. Tan, K. Ngo, S. Luo, G.Q. Lu, Proc. 2nd IMAPS Adv. Tech. Workshop Automotiv. Microelectron. Package, 2010, pp. 1–4.
[107] P. Panaccione, T. Wang, X. Chen, S. Luo, G.Q. Lu, Proc. 6th Int. Conf. Exhib. Device Package, 2010, pp. 1–5.
[108] H. Zheng, L. Xu, J. Calata, K. Ngo, S. Luo, G.Q. Lu, Int. Conf. Electron. Package (2011) 241–245.
[109] T. Ogura, M. Nishimura, H. Tatsumi, N. Takeda, W. Takahara, A. Hirose, Open Surf. Sci. J. 33 (2011) 55–59.
[110] G.Q. Lu, Applications: Recommended Heating Profiles, NBE Tech LLC, 9 July 2011, http://www.nbetech.com/application.shtml.
[111] J. Zhang, S. Xie, X. Wei, Y.J. Xiang, C.H. Chen, J. Power Source 137 (2004) 88–92.

[112] M. Yeadon, J.C. Yang, R.S. Averback, J.W. Bullard, J.M. Gibson, Nanostruct. Mater. 10 (1998) 731–739.
[113] S. Egelkraut, L. Frey, M. Knoerr, A. Schletz, Proc. 12th Electron. Package Tech. Conf., 2010, pp. 660–667.
[114] R. Dannenberg, E. Stach, J.R. Groza, B.J. Dresser, Thin Solid Films 379 (2000) 133–138.
[115] P.G. Sanders, J.R. Weertman, J.G. Barker, J. Mater. Res. 11 (1996) 3110–3120.
[116] M. Knoerr, S. Kraft, A. Schletz, Proc. 12th Electron. Package Tech. Conf., 2010, pp. 56–61.
[117] S.M. Bidoki, D.M. Lewis, M. Clark, A. Vakorov, P.A. Millner, D. McGorman, J. Micromech. Microeng. 17 (2007) 967–974.
[118] D. Wakuda, M. Hatamura, K. Suganuma, Proc. 6th Int. IEEE Conf. Polym. Adhes. Microelectron. Photonics, 2007, pp. 110–113.
[119] H. Schwarzbauer, US5893511, Siemens AG, 1999.
[120] A. Muza, Lead-free Solutions for High and Low Temperature Solder Interconnects, MSc thesis, Purdue University, 2009.
[121] J. Nadler, Taking the Heat: Silver–Diamond Composite Offers Unique Capabilities for Cooling Powerful Defense Microelectronics, Georgia Technology Research Institute, 9th July 2011, http://www.gtri.gatech.edu/casestudy/silver-diamond-composite-cooling-microelectronics.
[122] N. Heuck, G. Palm, T. Sauerberg, A. Stranz, A. Waag, A. Bakin, Mater. Sci. Forum 645/648 (2010) 741–744.
[123] D.E. Gray, American Institute of Physics Handbook, Thermal Expansion of Cu and Diamond, 9 July, 2011, http://www.calstatela.edu/academic/nuclear_physics/99012/thermal_expansion.htm.
[124] R.G. Munro, J. Phys. Chem. Ref. Data 26 (1997) 1195–1203.
[125] M.C. Stensberg, Q. Wei, E.S. McLamore, D.M. Porterfield, A. Wei, M.S. Sepuelveda, Nanomed 6 (2011) 879–898.
[126] B. Nowack, H.F. Krug, M. Height, Environ. Sci. Tech. 45 (2011) 1177–1183.
[127] Y. Mei, G.Q. Lu, X. Chen, S. Luo, D. Ibitayo, IEEE Trans. Device Mater. Rel. 11 (2011) 312–315.
[128] C. Gobl, US2007/0131353A1, Semikron Elektronik GmbH, 2007.